Space Launch System Base Heating Test: Experimental Operations & Results

Aaron Dufrene*, Manish Mehta†, Matthew MacLean‡, Mark Seaford§, Michael Holden**

CUBRC / LENS, Buffalo, NY, 14225
&
NASA Marshall Space Flight Center, Huntsville, AL 35811

NASA's Space Launch System (SLS) uses four clustered liquid rocket engines along with two solid rocket boosters. The interaction between all six rocket exhaust plumes will produce a complex and severe thermal environment in the base of the vehicle. This work focuses on a recent 2% scale, hot-fire SLS base heating test. These base heating tests are short-duration tests executed with chamber pressures near the full-scale values with gaseous hydrogen/oxygen engines and RSRMV analogous solid propellant motors. The LENS II shock tunnel/Ludwieg tube tunnel was used at or near flight duplicated conditions up to Mach 5. Model development was based on the Space Shuttle base heating tests with several improvements including doubling of the maximum chamber pressures and duplication of freestream conditions. Test methodology and conditions are presented, and base heating results from 76 runs are reported in non-dimensional form. Regions of high heating are identified and comparisons of various configuration and conditions are highlighted. Base pressure and radiometer results are also reported.

I. Introduction

Reusable solid rocket motors and hydrogen/oxygen rocket engines have been developed for subscale hypersonic wind tunnel tests of NASA's Space Launch System (SLS) vehicle in the LENS II shock/Ludwieg tube facility. SLS is composed of four RS-25D LOX/LH2 rocket engines in the core stage and two 5-segment solid rocket motors in the booster stage. SLS is designed to take NASA beyond low-earth-orbit for the first time in over forty years and the geometry of rocket motors are significantly different than previously flown systems. Convective base heating testing is one of a series of ground tests required to successfully develop this next generation rocket. Rocket motor plume interaction drives base heating and is extremely complex and difficult to simulate with modern computational fluid dynamic tools. Ground experiments of a 2% scale model operating near flight chamber pressures with flight-like propellant at duplicated flight conditions have been tested. These ATA-002 tests will help NASA MSFC in developing ascent plume induced thermal design environments for the SLS vehicle.[1]

The primary goal of the ATA-002 test program is to define the convective base heating environment. Experimental operations and non-dimensional results are described in detail over a wide range of conditions. Sub-scale solid rocket motor and core-stage engine performance and operation are discussed in Section II. Test conditions are discussed in detail in Section III including shock tunnel, Ludwieg tube, and altitude simulation operation of LENS II from 50-210 kft. Short-duration testing for base heating experiments is critical to achieving proper conditions for scaling to flight environments. Short-duration tests allow testing at or near flight-like conditions matching flight total temperatures and pressures, as well as rocket motor and engine chamber pressures and temperatures. Test hardware was designed to handle high-temperatures for short periods of time and reused with minimal refurbishment between tests. Test operations and timing of critical events such as firing the tunnel, motors and data collection are also discussed in

* CUBRC Senior Research Scientist, Member AIAA; dufrene@cubrc.org
† NASA MSFC Senior Research Scientist, Member AIAA; manish.mehta@nasa.gov
‡ CUBRC Senior Research Scientist, Member AIAA; maclean@cubrc.org
§ NASA MSFC Senior Research Engineer, Member AIAA; dr.c.seaford@nasa.gov
** CUBRC Vice President of Hypersonics, Fellow AIAA; holden@cubrc.org

Section III. Lastly, the non-dimensional heating and pressure results are reported in Section IV along with discussion of interesting trends identified during testing.

Figure 1 shows a schematic of the SLS vehicle with regions of interest in the base region labeled in the bottom half of the figure. The model designed for these base heating studies can be configured with or without the solid rocket boosters attached. The configuration with the boosters attached is referred to as the Full-Stack configuration and the configuration without boosters is referred to as the Core-Stage. A photograph of both configurations installed in the LENS II tunnel is shown below in Figure 2.

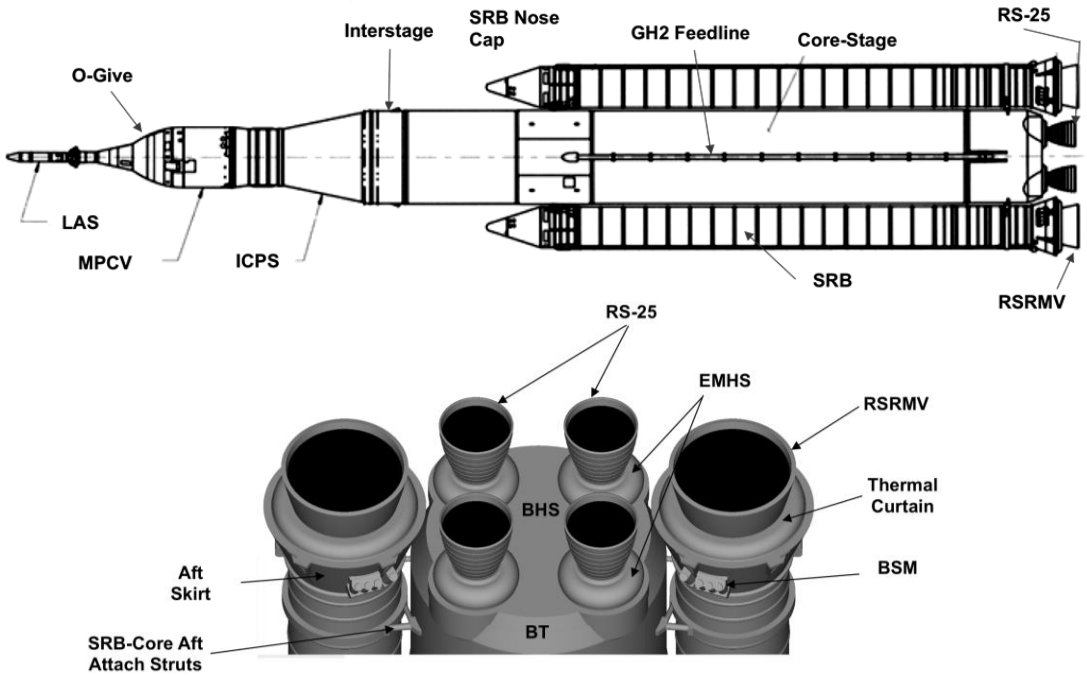

Figure 1. Schematic of SLS-10005 (top) and base components (bottom)

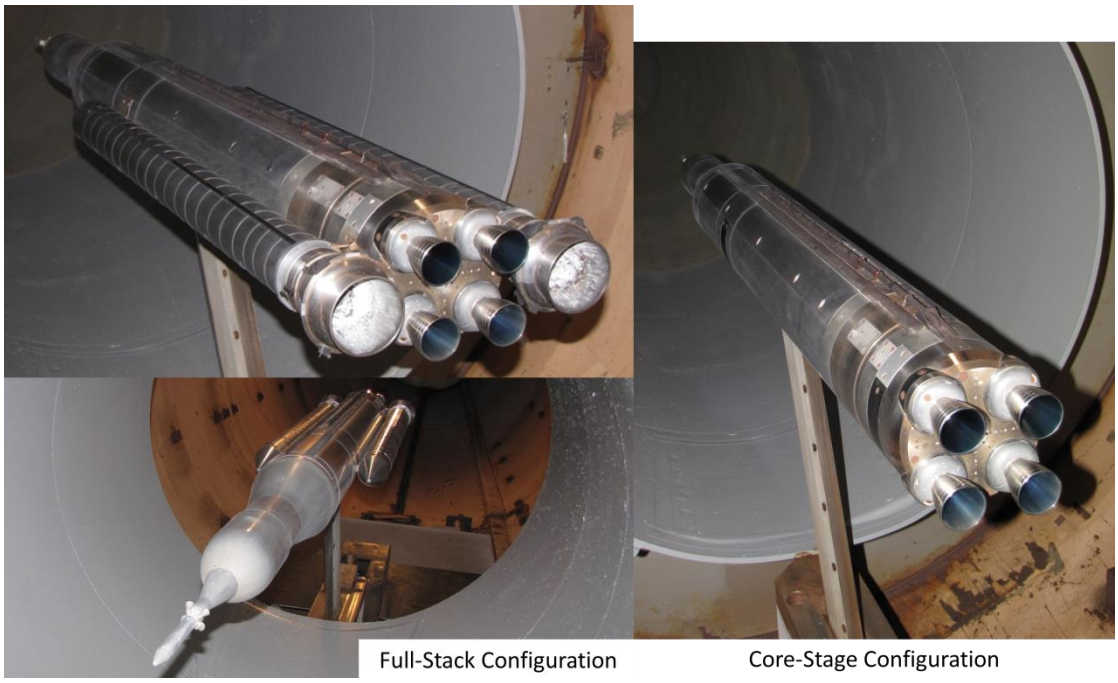

Figure 2. Photographs of 2% SLS Base Heating Model (Core-Stage & Full-Stack Configurations) in LENS II

II. Rocket Motor/Engine Development & Performance

The four hydrogen/oxygen engines are ported from a central combustor to minimize thrust/pressure mismatches and to simplify the model propulsion system. The central combustor is designed to operate at full-scale pressure up to approximately 2,900 psi, however, throat erosion at the higher pressures limited typical operating pressures between 2,300-2,700 psi. Gaseous hydrogen and oxygen charge tubes are pressurized up to 6,000 psi depending on the test conditions. During the test, gases are fed through flow-control venturis that set the oxidizer to fuel mass ratio (O/F) ratio to 6, and constant pressure is maintained through long, constant-diameter charge tubes. Gas flow is initiated by opening fast-response solenoid valves and the ignition source is a glow plug. The central combustor reaches steady state engine pressure in less than 20ms from sending the valve triggering signal. Specific details of engine performance and development are reported in Ref. [2].

The solid rocket motors use an ammonium perchlorate/high-aluminum-loaded solid propellant grain that is analogous to the RSRMV propellant. Thin cylindrical propellant castings are used to ensure even burning and achieve steady chamber pressures. The ignition source is a hydrogen/oxygen torch that adds less than 2% water to the combustion products, which is already dominated by water. Other ignition sources did not prove fast enough to get the solid rocket motors up to full, steady pressure within 30ms. These motors operate from 100-720psi. Specific details of motor performance and development are reported in Ref. [3].

Chamber pressures versus altitude are plotted below in Figure 3. Core engine chamber pressures for the nominal configurations/conditions are shown in dark blue with solid rocket booster chamber pressures shown in red and pink. For reference, the flight design chamber pressures are shown with solid green and dashed green lines for the core engine and solid rocket motors, respectively. In order, to reuse throat hardware multiple times core-engine operation pressure was reduced, so the solid rocket motor chamber pressures were dropped correspondingly. Previous base heating studies were tested at half full-scale pressure levels, so those values from the Space Shuttle 19-OTS test program are also shown for reference.

Figure 4 shows nozzle lip/exit pressure to freestream pressure ratio (P_{lip}/P_{inf}) versus altitude compared to flight design conditions for both the core engine and solid rocket motors. This ratio is critical to preserving plume expansion and the plume-plume interaction physics, so freestream pressures were reduced the same percentage as chamber pressures to preserve this ratio. P_{lip} is a calculated value based on the engine chamber pressure and nozzle expansion ratio, but P_{inf} is derived from tunnel measurements. In all cases, this pressure ratio is preserved except for a minor deviation at 140 kft where solid rocket booster chamber pressure drops significantly. Solid rocket motor fuel was designed to match RSRMV properties as discussed above, and core engine was designed to operate with an O/F ratio of six. Figure 5 plots O/F ratio versus P_{lip}/P_{inf} for the key test points. O/F ratio was determined from venturi section pressures and was at or very near target for all tests as shown.

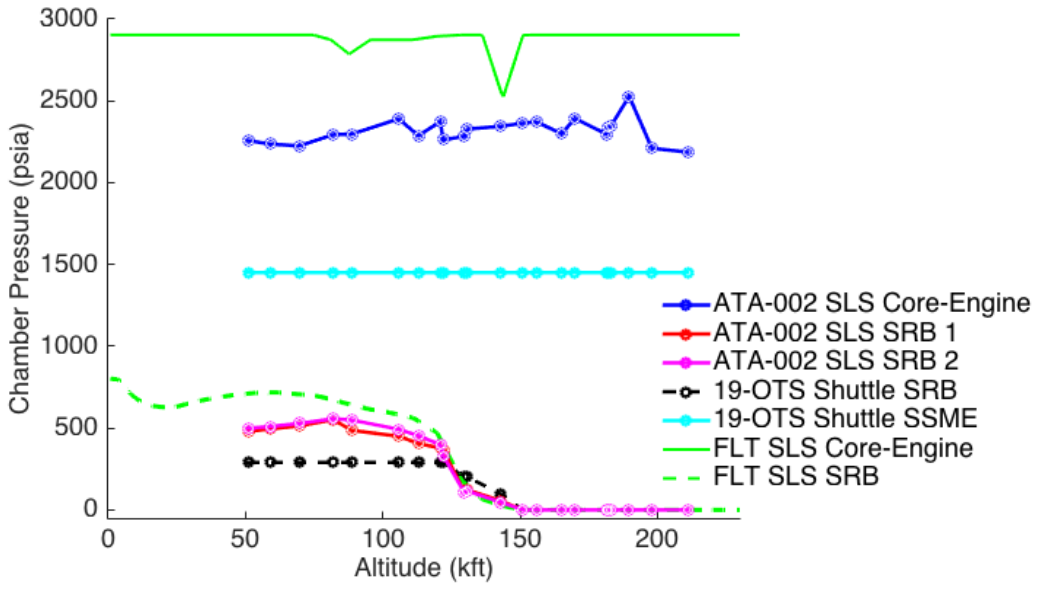

Figure 3. Chamber Pressure vs. Altitude for ATA-002 SLS Base Heating Model Compared with SLS Design Requirements and Space Shuttle 19-OTS Base Heating Model

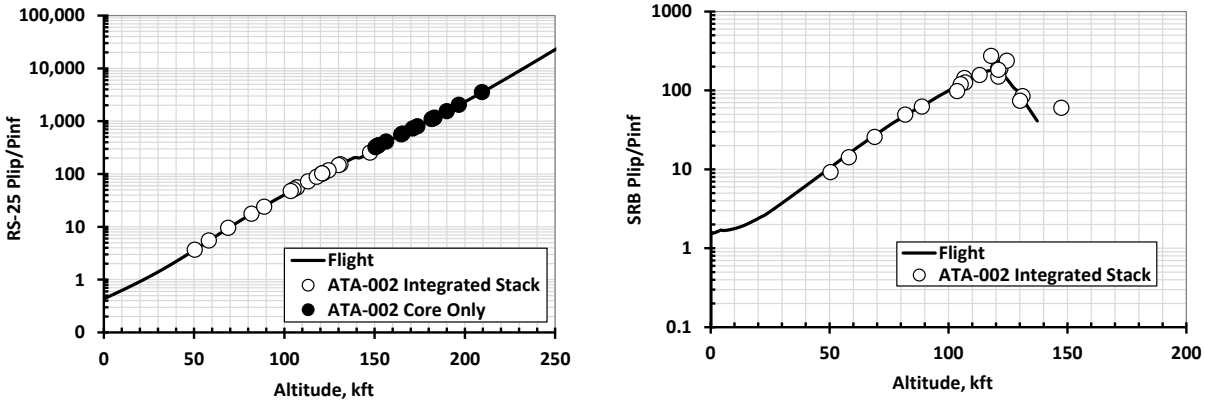

a. Core engine P_{lip}/P_{inf} vs. altitude

b. Solid rocket motor P_{lip}/P_{inf} vs. altitude

Figure 4. Scaled Rocket Engine and Rocket Motor Performance Compared to Flight Design Environments

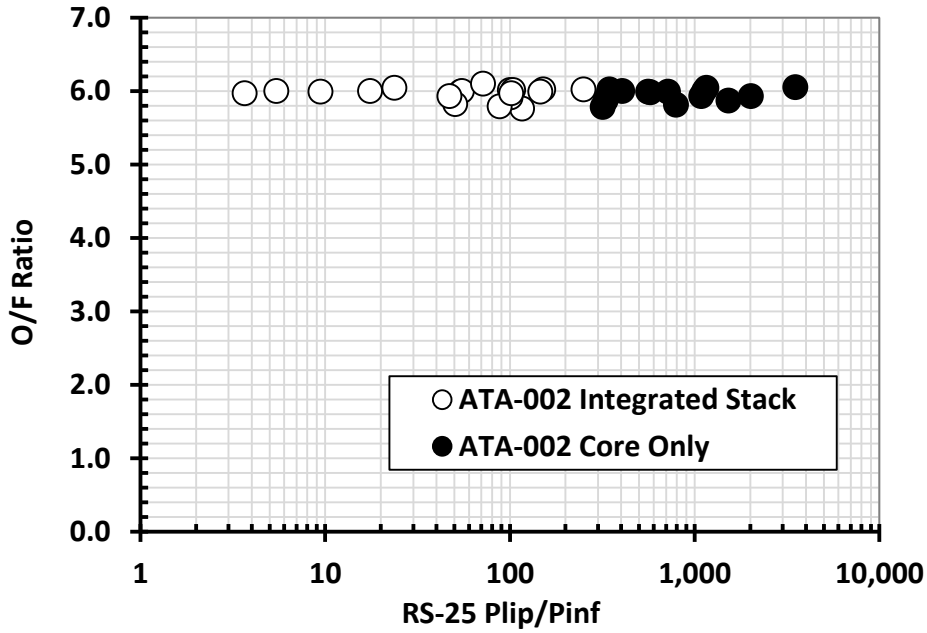

Figure 5. Oxidizer to Fuel Ratio vs. P_{lip}/P_{inf} Ratio

III. Instrumentation and Test Conditions

The primary goal of the ATA-002 test program is to define the SLS base heating environments from 50-200 kft. Heat transfer measurements supplemented with pressure and radiometer measurements are made in the base region to define the plume induced heating environments across a large range of altitudes and Mach numbers. Figure 6 shows the instrumentation layout for the base heating tests. Depending on the configuration for a specific run or the stage of the test program active gauge count varied from run to run. 185 total heat transfer gauges were available, as well as seven radiometers and 37 external pressure gauges and ten internal pressure gauges. The red circles in Figure 6 represent thin-film heat transfer instrumentation, and orange circles represent fast-response thermocouples which are also used to determine heat-flux, so those gauges are included in the heat transfer gauge count of 185. The purple radiometers are hard to distinguish from the red dots, but they have an additional circle around them. Limited forebody instrumentation was installed as shown in the figure with some additional gauges located along the full length of the cylindrical part of the Core-Stage, but instrumentation was overwhelmingly concentrated on the aft end of the model.

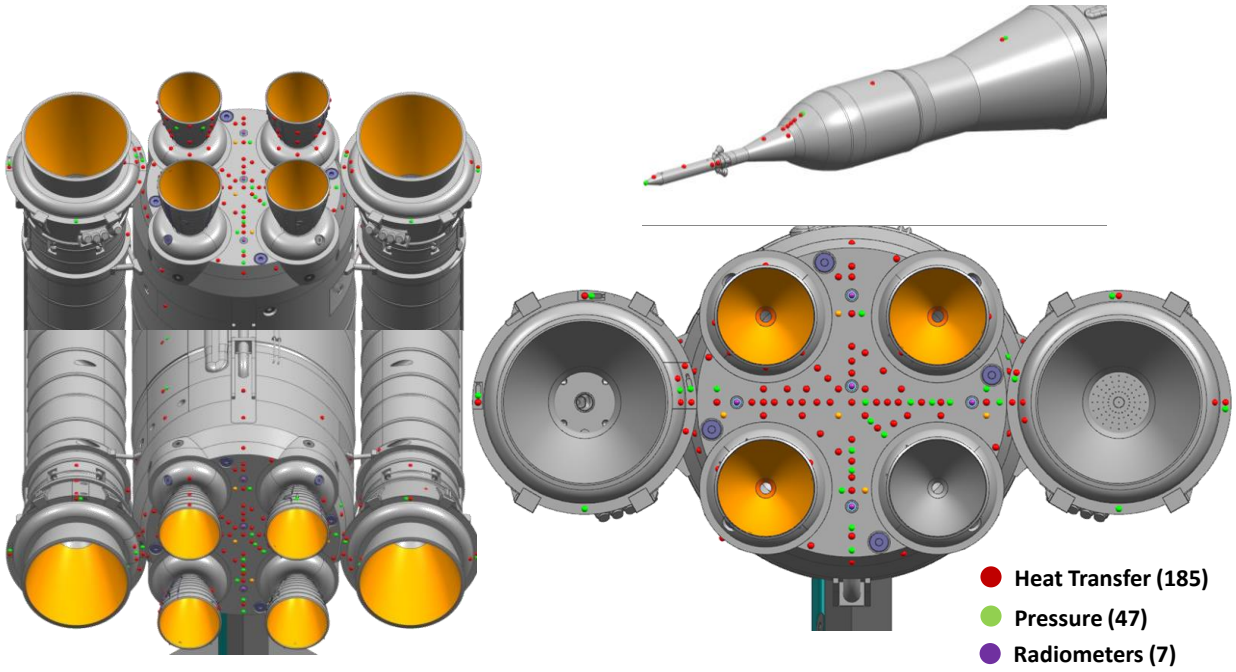

Figure 6. SLS Base Heating Model Instrumentation Layout

For these studies we employed thin-film heat transfer instrumentation similar to those designed at Cornell Aeronautical Laboratory (CAL) in the late 1950s and refined over the past 55 years. The platinum thin-film heat transfer instrumentation employed in these studies have proven to be the most accurate measurement technique in supersonic and hypersonic test facilities, and the small size of the sensing element coupled with the insulating substrate make them ideal for a high resolution measurements CUBRC has calculated the accuracy of the heat transfer measurement to be ±5%. The thin-film heat transfer gauge is a resistance thermometer that measures the local surface temperature of the model. The theory of heat conduction is used to relate the surface temperature history to the rate of heat transfer. Since the platinum resistance element has negligible heat capacity, and hence negligible effect on the Pyrex surface temperature, the gauge can be characterized as being homogeneous and isotropic with properties corresponding to those of the Pyrex.[4, 5] Furthermore, because of the short duration of the tests, the Pyrex can be treated as a semi-infinite body. Reduction of the surface temperature history to imposed heat flux is accomplished by using the well-known Cook-Felderman technique.[6]

Internal engine and motor pressures are measured with PCB 111 style pressure gauges. These piezoelectric gauges have micro-second response times with thermal protection, acceleration compensation, and strong shock protection. A thin coat of RTV is installed on the gauge face to improve thermal protection. Model external surface pressures were measured using Measurement Specialties EPIH piezoresistive pressure gauges. The piezoresistive gauges are small, have good shock protection, fast response time, and good output sensitivity at the low pressures required for these tests.

Two types of radiometers were employed. One was simply a standard thin-film gauge with a thin CVD diamond window installed over the top of the gauge. There were three of these radiometers for the sole purpose of determining the radiative component of heating measured by the standard surface thin-film gauges. Radiative component measured was small relative to the convective heat transfer in almost all cases. Additionally, custom Vigo IR radiometers were used to measure the IR radiative heating in the 2-11 micron range. A PVM-10.6 detector with custom packaging in a TO18 can with BaF_2 window and steel housing was used. These Vigo radiometers were calibrated using a blackbody source and installed nearly flush with the base plate having a wide view angle of approximately 70-degrees.

Scaling 2%-model-scale heat transfer data to flight is complicated by the fact that gas temperature and gas composition is not known or directly measured. Typical aerothermal scaling is not difficult, because the tunnel freestream conditions are well defined, but plume interactions are poorly understood. This was a large source of uncertainty for previous Space Shuttle base heating studies[7, 8]. There were two approaches to determine gas temperature in previous testing. The first method relied on platinum-rhodium thin-wire resistance temperature

detectors (RTDs)[9]. These are minimally-heated hot-wire probes that heat up when exposed to the rocket exhaust. Gas properties are unknown, so two different length wires and a complex analysis is required to reduce the temperature data. This measurement is intrusive and often had uncertainties of several hundred degrees Rankine. The second method utilized a heated base plate and high-temperature thin-film heat flux instruments[10]. As the wall temperature increases heat transfer decreases linearly to the gas recovery temperature. Therefore, from tests performed with the base plate heated to several different temperatures, gas temperature can be extrapolated. This method is nonintrusive, but has downsides including the need to perform several runs to obtain one gas temperature measurement, and the need to use high-temperature instrumentation which limits the instrumentation options. These measurements require a complex setup, and other parts of the model such as nozzle or central combustor can be inadvertently heated which may affect measured heat transfer. Also, as the wall is heated heat transfer goes down and the signal-to-noise ratio of the heat transfer measurements is reduced. The importance of this base gas temperature measurement, and the high uncertainty reported in previous programs motivated the development of an instrument that was based on tunable diode laser absorption spectroscopy (TDLAS) which shows promise as a more accurate, non-intrusive measurement of path-averaged base gas temperature. From TDLAS measurements, time-resolved, path-integrated base-region gas temperature is obtained with information about pressure and tracer species concentration also available. Water is a primary exhaust species in many hot-fire rockets including SLS, and is used as the spectroscopic tracer. Details of the measurement TDLAS instrument development and calibration are reported in Ref. [11]. Test results are reported in Ref. [12] and show a large range of gas temperatures and velocities depending on the test conditions.

SLS base heating studies are being executed in the LENS II shock and Ludwieg tunnel. LENS II is capable of operating over a Mach range of $2.7 \leq M_\infty \leq 9.25$ and pressure altitudes of sea-level $\leq H \leq$ 200kft (Figure 7). LENS II can operate as a throatless Ludwieg tube[13] with total temperatures up to 400K at Mach 2.7, standard Ludwieg tube with total temperatures up to 500K from Mach 3.5-7, and flight matching total temperatures up to Mach 8 as a reflected shock tunnel. Base heating test freestream conditions are designed to match flight conditions exactly, as opposed to typical scaled Reynolds number testing. A small correction to freestream pressure is made when operating the engines at less than 100% of the full-scale value. This is done to preserve the plume expansion and interaction region which has a first-order effect on base heating levels. Model boundary layer conditions do not match flight-scale, but analysis indicates boundary layer state and size are not drivers in base heating levels. LENS II is also used as a vacuum chamber for altitude simulation only up to 210 kft.

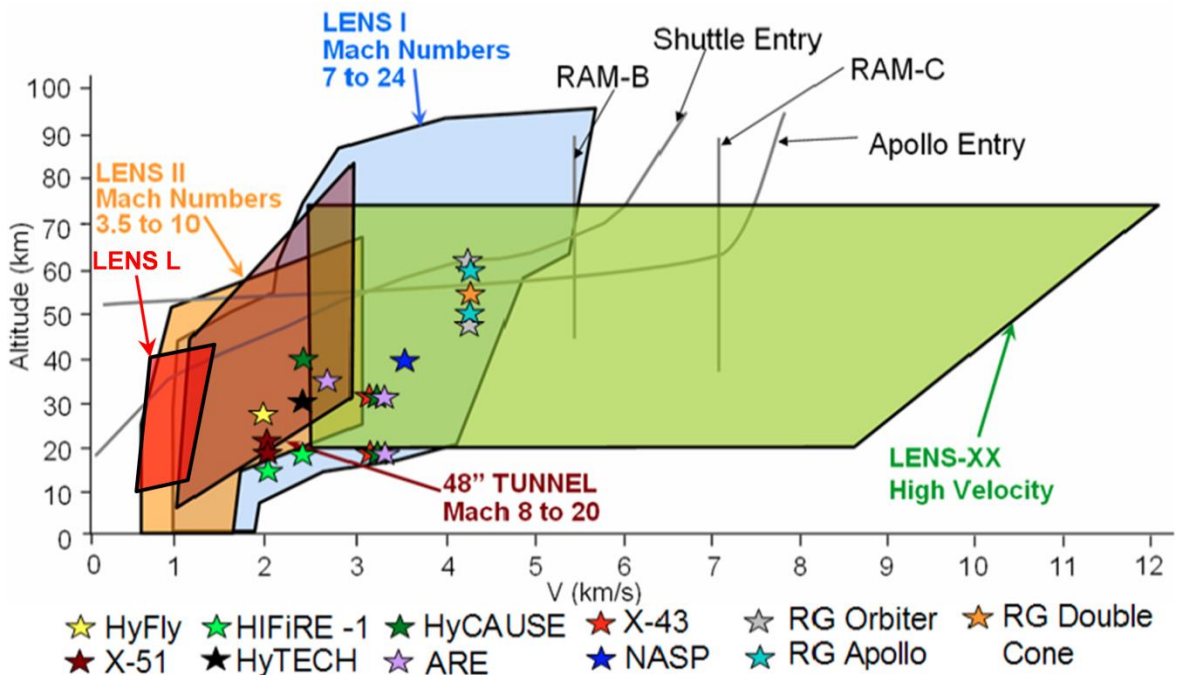

Figure 7. Velocity/Altitude Capabilities of the LENS Shock Tunnels and Expansion Tunnel

LENS II as-run test conditions compared to the flight design trajectory are shown below in Figure 8. Figure 8a shows Mach number versus altitude with fairly good agreement. The minimum facility Mach number is 2.7, so at the

lower altitudes there is a little deviation, and at the higher altitudes freestream pressures are so low, that Mach numbers were biased high a little to maintain the proper P_{lip}/P_{inf} ratio discussed above. Figure 8b & d show dynamic pressure versus Mach number and altitude, respectively. Some variation of dynamic pressure was explored, but most test points were ran to match the flight trajectory as close as possible as shown in Figure 8d. Total temperature versus altitude is shown in Figure 8c. Total temperature drives freestream temperature and velocity, so it is an important parameter when considering aerothermal measurements. Very good agreement up to 120 kft is observed, but above 120 kft the freestream pressures were so low that it was necessary to drop the tunnel total temperature slightly to achieve good tailored test conditions. Facility refinements could be made in the future to allow duplication up to the 160 kft condition.

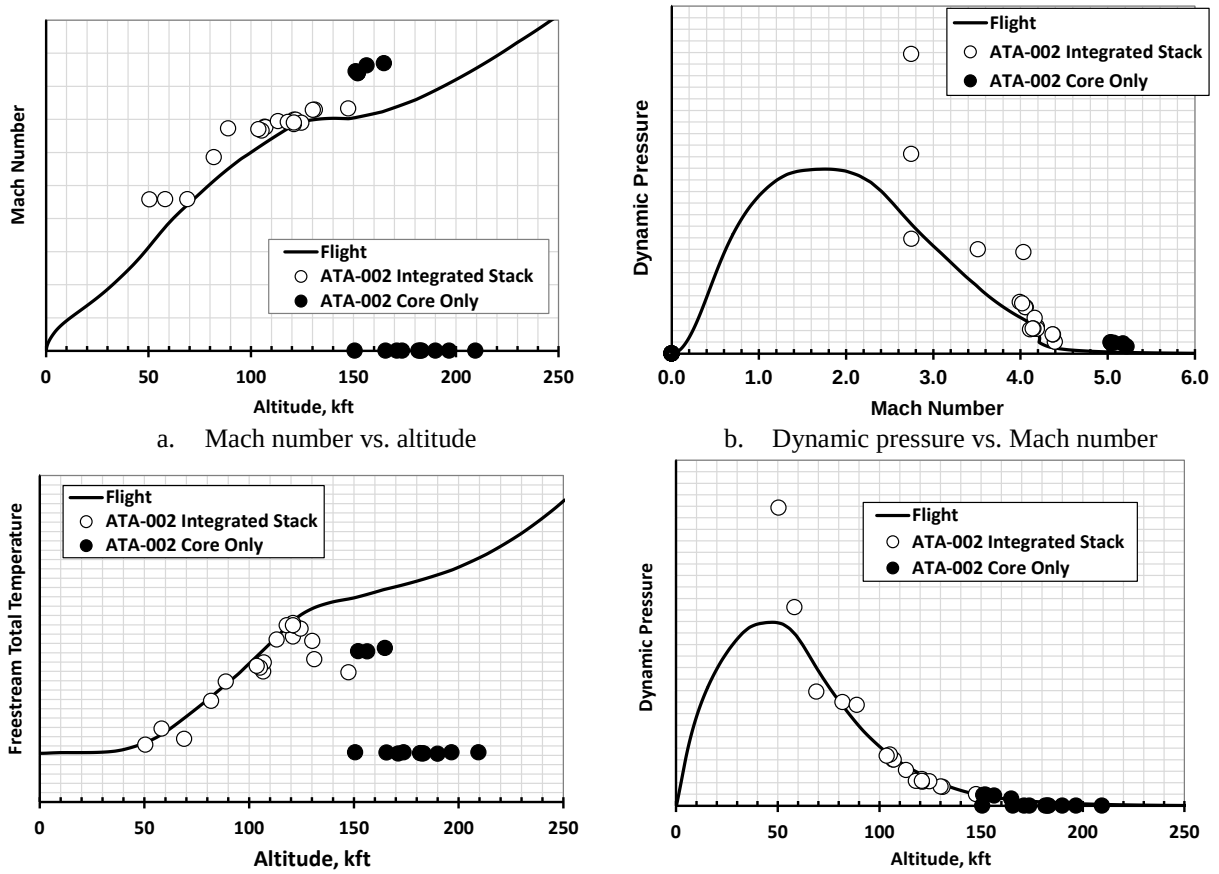

a. Mach number vs. altitude

b. Dynamic pressure vs. Mach number

c. Total temperature vs. altitude

d. Dynamic pressure vs. altitude

Figure 8. Wind Tunnel Test Conditions Compared to Flight Design Environments

Nominal test points were all completed at zero angle-of-attack and yaw with no nozzle gimballing. Deviations from nominal test points included dynamic pressure variations and chamber pressure variations to evaluate scaling effects. Model geometry changes included several engine out cases where one of the RS-25 nozzles was blanked off, as well as angle-of-attack runs at 4-degrees and gimballed nozzle runs where the RS-25 nozzles were gimballed 2-degrees and RSRMV nozzles remained fixed at zero degrees.

IV. SLS Base Heating Test Results

Short-duration testing is critical to model and instrument reusability in these hot-fire base heating studies, so test time is long enough to obtain high-quality steady measurements, but short enough to ensure reusability of the hardware. A typical timing sequence is shown in Figure 9, showing that the flow over the model starts just prior to, or coincident with, the ignition of the solid rocket motors. Compared to the core stage, the solid rocket motors take longer to start and become steady so the core-stage engine firing is delayed by 10-15ms. All engines are firing for a

steady-state test time of ~40-50ms, at which point the core-stage engines shut down immediately, and solid rocket motors begin to slowly shut down. Tunnel test time is up to 300ms at lower velocity/lower Mach number conditions and as short as 30ms at high velocity/Mach number conditions, so repeatable and accurate timing of rocket motors and tunnel operation has been demonstrated and is critical to successful base heating studies. Pitot traces for both high and low Mach number conditions are shown in Figure 9. In addition to ensuring tunnel and rocket motor steady state operation, additional parameters are considered such unsteadiness of the base flow, proper O/F ratio during the steady-state window.

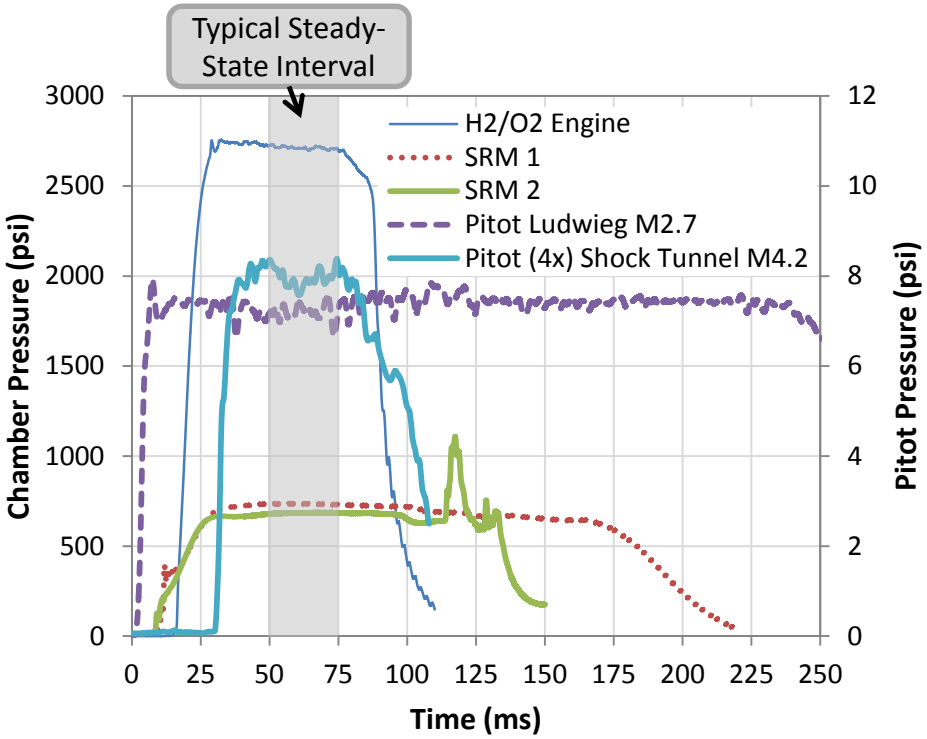

Figure 9. Typical timing sequence for 2%-scale SLS base heating hot-fire testing

Figure 10 shows all of the aft-body heating data for all of the fully-instrumented runs plotted against freestream pressure. Runs 1-18 were development runs with limited instrumentation and are not included in the base heating results reported in this work. In Figure 10, the x-axis can be thought of as altitude with pressure values in reverse order on a log-scale such that increasing altitude is shown from left to right. High pressure/low altitude runs resulted in relatively low base heating values with peak heating at approximately 120 kft, followed by a reduced by relatively constant heating at higher altitudes Each run is depicted with a different symbol and there are several overlapping cases where repeat runs were completed or off nominal cases were evaluated. All heat transfer data are shown without units, but run axes are consistent, so that qualitative observations can be made. All data is reported in raw form without scaling values based on chamber pressure or adjusted for radiative heating or any other parameters. Scaling results does not change the trends or results presented in this work, but it is important in defining the convective heating environments for SLS which is reported in Ref. [1].

Computational fluid dynamic (CFD) analysis was used to support the SLS Base Heating studies in several different ways. CFD simulations were run using NASA's DPLR code[14]. Initially, CFD was used to evaluate scale-size, model placement in the tunnel, angle-of-attack limits, and tunnel wall effects. CFD was also used to design and place the model sting support such that the influence of the sting was near negligible in the base region [15]. Sting design is an important design feature for base studies that is often ignored. The Space Shuttle base heating Ludwieg tube testing for instance had a sting support that ran most of the length of the external tank and almost as wide as the external tank. The Shuttle itself sits on top of the external tank, so the sting likely has less influence on the orbiter's base, but sting size is still an important consideration.

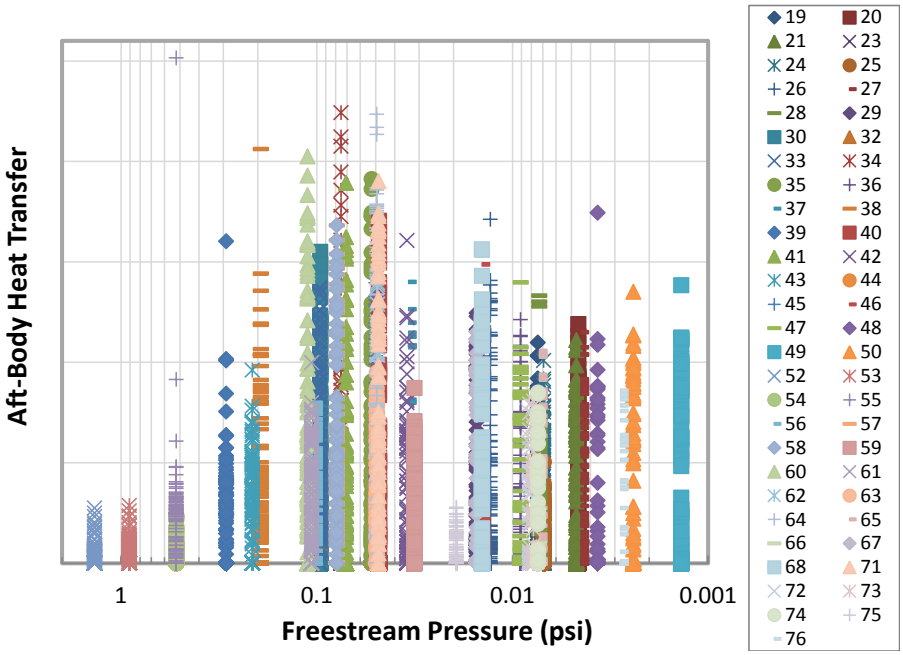

Figure 10. Aft-Body Heat Transfer vs. Freestream Pressure for All Fully Instrumented Cases

CFD is also used to help interpret test data. A primary example of this is to compare forebody surface pressure and heat transfer predictions. Excluding interactions with protuberances and plume induced flow separation effects, CFD predictions of surface pressure and heat transfer should match test data fairly well. CFD solutions for all altitudes and Mach numbers were computed for both turbulent and laminar boundary layers such as the 70 kft example in Figure 11. These solutions are used to verify surface pressure distribution and help determine the state of the boundary layer over the model. The 70 kft forebody pressure predictions match experimental data well, and heat transfer values agrees better with the laminar CFD prediction indicating the boundary layer is likely laminar. The 70 kft condition is one of the higher Reynolds numbers tested, and all other cases agree more closely with the laminar boundary layer calculations as well.

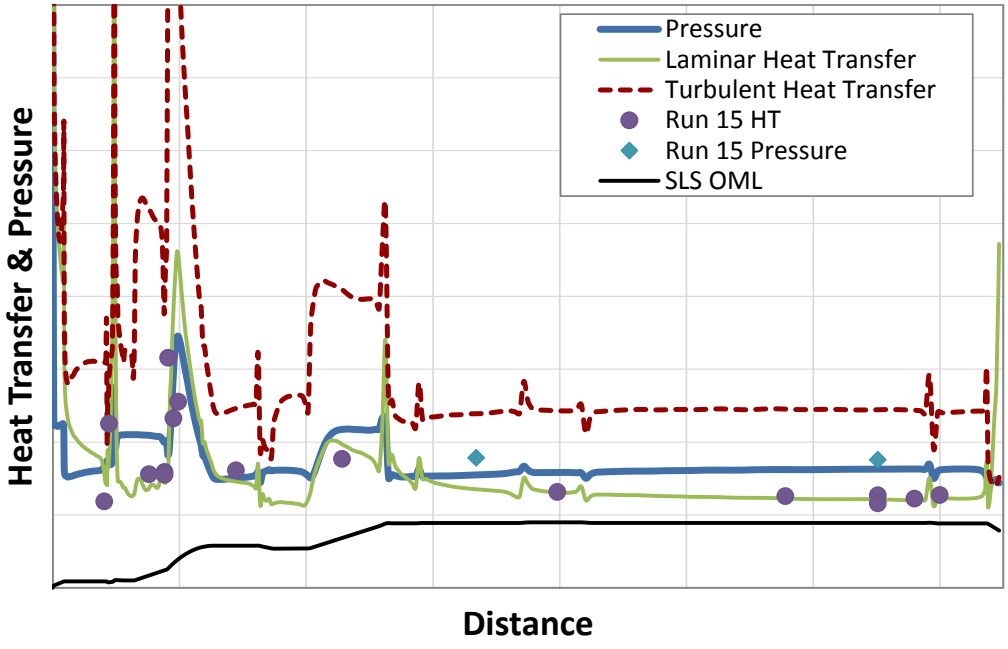

Figure 11. Surface Aerothermal Predictions & Measurements for 70kft Condition

More complex CFD simulations were performed for several altitudes for the Core-only configuration with freestream rocket engine flow. In these cases, several simplifications were made – the vehicle is computed $1/8^{th}$ by symmetry, smooth OML was considered, the core engine gas is assumed to be fully burned in the combustion chamber such that the product gas composition is water (H_2O), and the freestream Air is assumed to be of inert composition. The simulations were composed of approximately $8x10^6$ structured grid cells and calculation convergence was monitored until the heat flux field over the base region stabilized and ceased to change significantly as the calculation was advanced in time. The diverging section of the RS-25 nozzle interior is included in the simulation to approximate the boundary layer growth on the inner wall surface starting from just downstream of the throat. Despite these approximations, it is noted that these CFD simulations shown in Figure 12 and Figure 13 reproduce much of the behavior observed in the experiments for these runs. Experimental test data from Runs 26 and 32 are provided below (Figure 14) for Core-only firing at 150 and 100 kft conditions, respectively. Most importantly, the CFD reproduces the qualitative increase in heat flux observed for Run 26 (150 kft) compared to Run 32 (100 kft). The simulations predict that this effect is roughly proportional to the entrainment of hot water vapor from the core motor into the base region. At the lower altitude (higher freestream density), cooler air from the freestream dilutes the plume gas and reduces heat flux. The hot region at the center of the base between the nozzles and the rapid decrease toward the outer part of the base region are also captured. Base pressures show reasonable agreement with the measurements too. Finally, of primary concern is the heating on the inner portion of the Engine Mount Heat Shield (EMHS) surrounding each nozzle (e.g. at the 45^O position of the ring). This is particularly emphasized also at the high altitude where plume dilution is minimized. It can be observed from the CFD solutions that the narrow region of increased heat flux on the EMHS is expected to be nearly as high or potentially even higher than the peak heating of the center of the base depending on the altitude. Experimental results of EMHS heating are discussed later in this section, but in general are in good agreement. Run 26 had no boosters attached, but they were attached for Run 32, so heat transfer values for y values greater than 0.5" are not included in the Run 32 radial distribution plots shown in Figure 14. Both vertical and horizontal instruments were included for Run 26. CFD magnitudes and trends compare well with measured data. At the lower altitude Run 32 the pressure profile is nearly flat and the difference between center heat transfer and outboard heat transfer is much smaller. Likewise, at the higher altitude Run 26 the pressure and heat transfer values vary significantly from the peak at the center to much lower values near the edge of the base. The width of the heat transfer distribution in both cases is under predicted, but the trend is in agreement and peak values are close to measured values.

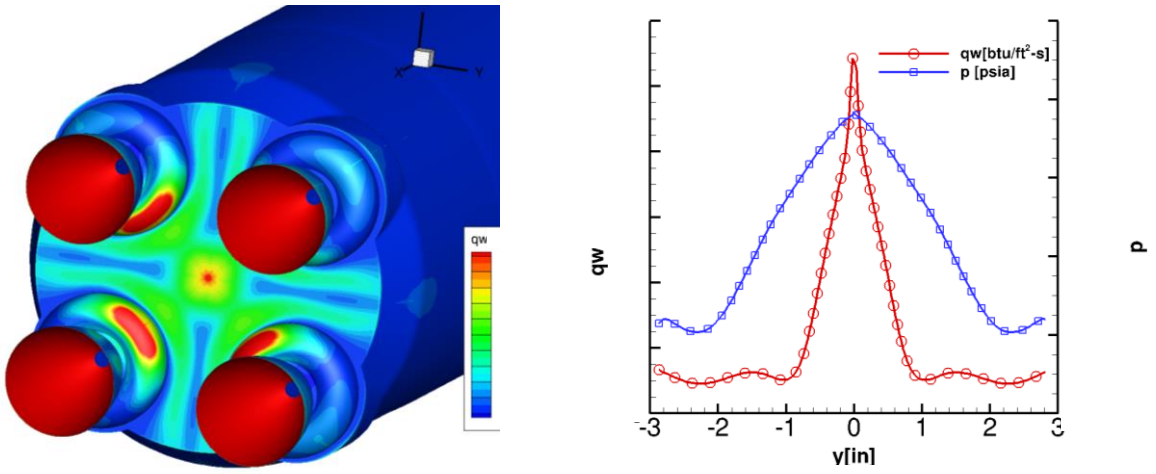

a. Heat Flux Contours b. Line cuts across symmetry plane

Figure 12. CFD Calculation of Core-only configuration at 150 kft conditions (Run 26)

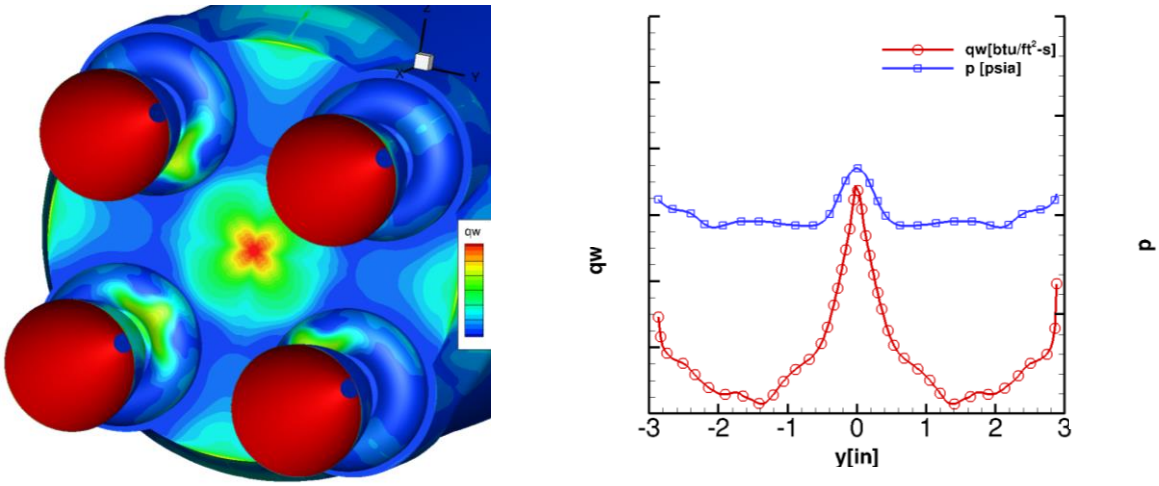

a. Heat Flux Contours b. Line cuts across symmetry plane

Figure 13. CFD Calculation of Core-only configuration at 100 kft conditions (Run 32)

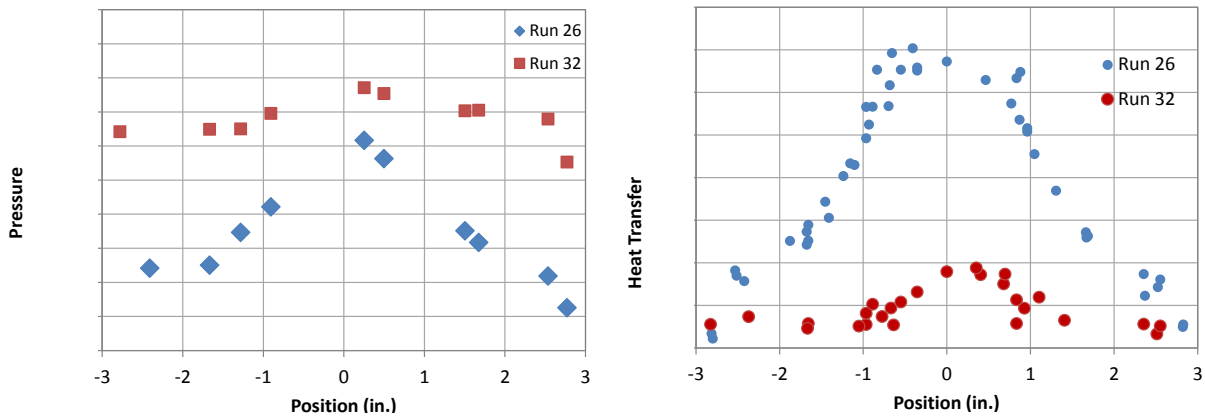

a. Pressure vs. Radial Distance b. Heat Transfer vs. Radial Distance

Figure 14. Core-only Aerothermal Test Data for Runs 26 (150kft) and 32 (100kft)

Region specific heat transfer values are highlighted in Figure 15. These plots are very similar to Figure 10 with the x-axis representing freestream pressure or altitude. All scales are the same, so that comparisons can be made easily. Base center heat flux peaks at the pressure corresponding to 120 kft test condition where rocket boosters are still firing. After 120 kft solid rocket motor chamber pressure tails off (see Figure 4b) and base center heat flux is reduced. The base center heat flux levels off to approximately half of the peak value and remains relatively constant up to the highest altitude tested. The lower dispersions observed for base center heat flux values are for off-nominal cases. Figure 15b shows the heat flux on the engine mount heat shields. In many cases, these values are higher than the base center values, and the higher heating levels persist out to the highest altitudes tested. Figure 15c shows the solid rocket motor base heat transfer values with similar trends, however, heating at the higher pressures is higher than that of the core base plate, and the reverse is true at lower pressure conditions. Figure 16 shows the core base plate heat transfer distribution for all nominal cases from 50-210 kft. Run numbers in the legend are replaced with the nominal run altitude, and the x-axis is distance from the base center. Peak base heating occurs at the base center in all cases except the 130kft conditions where solid rocket motor pressure is tailing off.

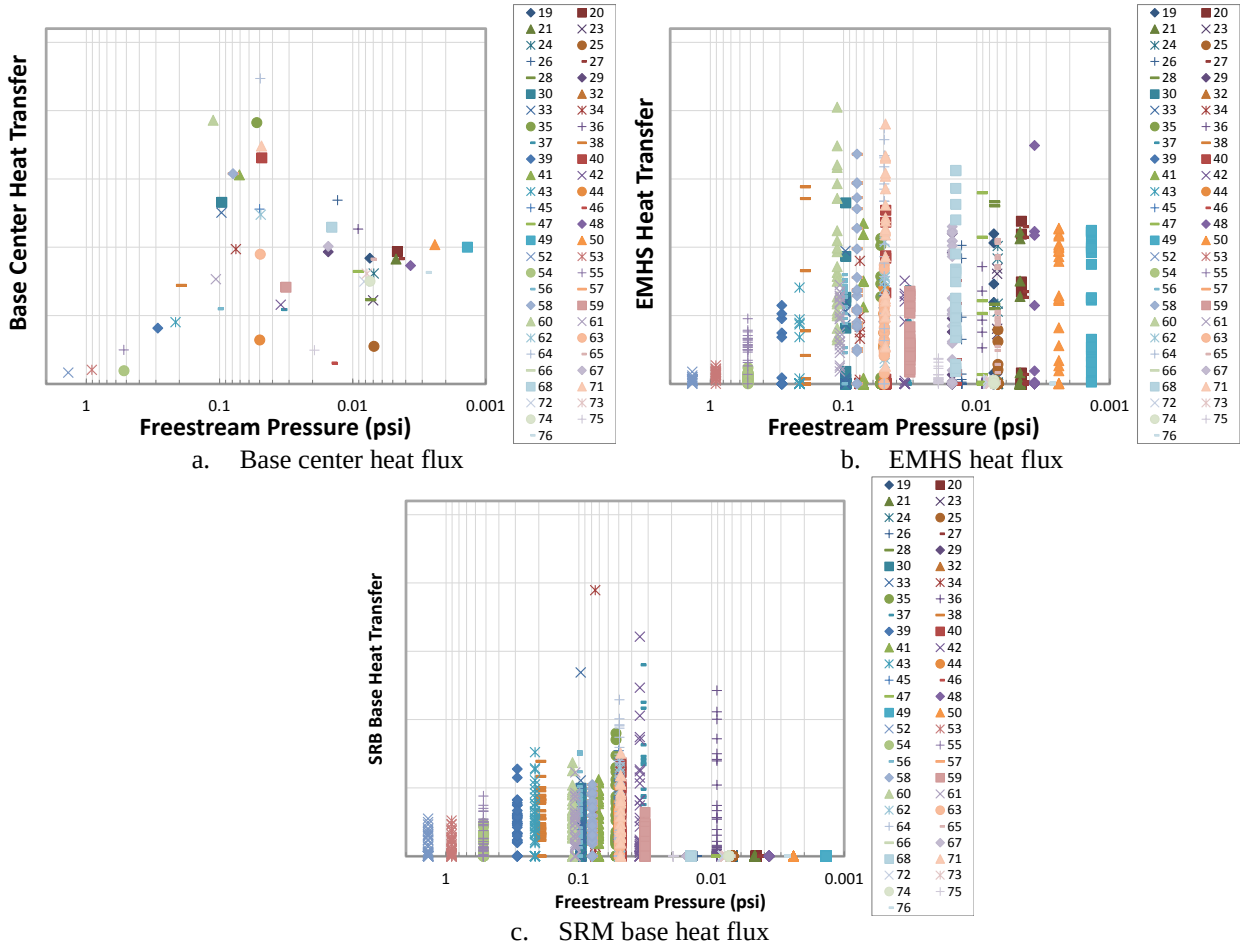

a. Base center heat flux

b. EMHS heat flux

c. SRM base heat flux

Figure 15. Region Specific Aft-Body Heat Transfer vs. Freestream Pressure

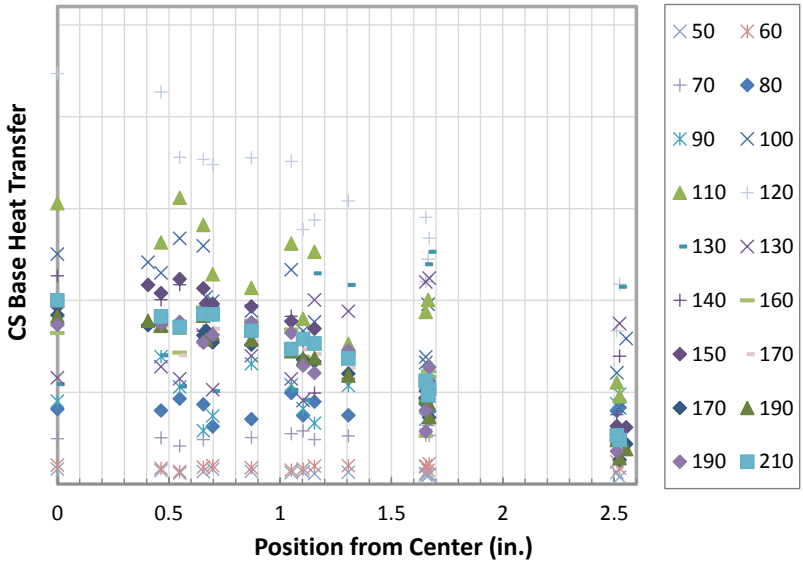

Figure 16. Base Heating Distribution Across Core-Stage Base Plate at All Nominal Conditions from 50 kft-210 kft

Freestream flow effects were not parametrically investigated over a large range of conditions since in most cases freestream conditions could be duplicated, however, Figure 17 shows base heating distribution for five different tests with and without flow and at various total temperatures and pressures. Heat flux measurements at and above 170 kft are nearly constant without flow, so for discussion purposes the blue diamonds in Figure 17 represent 170 kft simulated altitude test only and other runs will be compared to that run configuration. The cold flow Ludwieg tube test at the same simulated altitude actually shows significantly lower heating results than the altitude only simulation, suggesting cold flow base heating studies may under predict base heat flux values. Both cases at 150 kft and 160 kft with higher total temperatures fall short of the total temperature required to duplicate flight conditions at those altitudes. Additionally, base heating for the 150 kft case with warm freestream flow is significantly higher than the no flow case at 150 and 170 kft. More parametric testing is required to draw clear conclusions, but there is evidence to suggest that freestream conditions play an important role in base heating characterization.

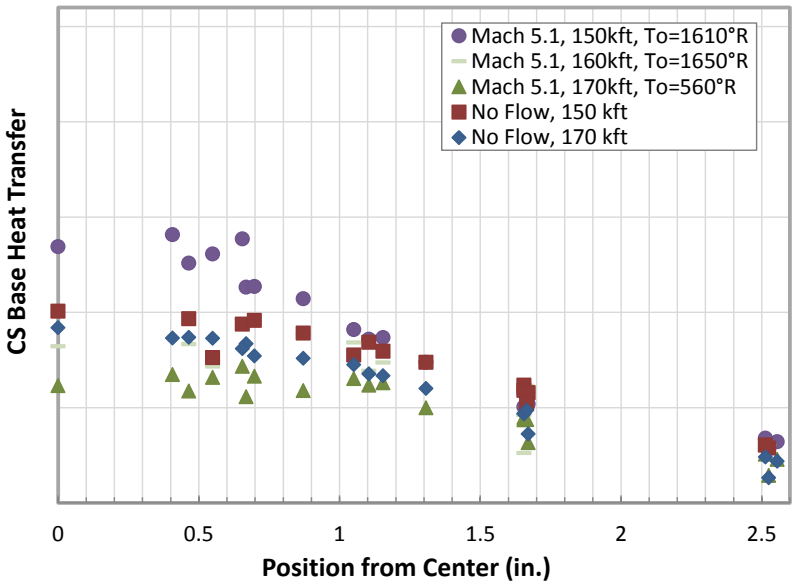

Figure 17. Freestream Flow Effects on Base Heating Distribution Across Core-Stage Base Plate

In order to evaluate scaling procedures several runs at reduced chamber pressures were made. Figure 18a shows the core base heating distribution for core only tests at various chamber pressures and a fixed test section pressure at a simulated 170kft condition. The 80% scale chamber pressure (Pc) case has a scaled test section pressure to maintain the appropriate P_{lip}/P_{inf} ratio, but all other cases have the same initial test section pressure. Heat transfer drops dramatically with chamber pressure as expected, and this relationship is needed when scaling base heating results at reduced chamber pressures to flight environments. Figure 18b shows a similar plot for the full-stack configuration, so both SRM and core stage engine pressures were reduced. Test methodology was different for these series of tests such that the appropriate P_{lip}/P_{inf} ratio was maintained for all tests, and this resulted in a more linear relationship between chamber pressure and base heat transfer. It is possible that in the fixed altitude core only cases that the flow dynamics are changing as the P_{lip}/P_{inf} ratio decreases resulting in a slightly different scaling trend than might otherwise be predicted by maintaining the P_{lip}/P_{inf} ratio, but more scaling data would improve this understanding.

Surface heat flux interpolations are shown in Figures 19 and 20. The interpolations were done with a relatively small amount of gauges with a nearest point fit, and no assumptions of symmetry or radial geometry were made to smooth out the interpolations, but these plots are still useful to discuss the flow physics of these conditions. In Figure 19, it clearly shows the hot spot in the middle of the base with a line of high heating directed towards the engine mount heat shields. EMHS heating decreases radially moving away from the center. Solid rocket motor thermal curtain shows the highest heating inboard and similar to that of the core base periphery. RS-25 nozzle lip shows relatively high heating inboard with decreased heating closer to the base and away from base center. Figure 20 shows the interpolation of the base plate only for the 120 kft nominal case, 4-deg angle-of-attack case, and the 2-deg RS-25 nozzle gimbal case. All interpolations have the same scale, so it is clear the nominal configuration has the highest heating. Additionally, off-nominal cases have larger asymmetries than the nominal case. These observations apply to engine out cases and other off-nominal cases at other altitudes as well.

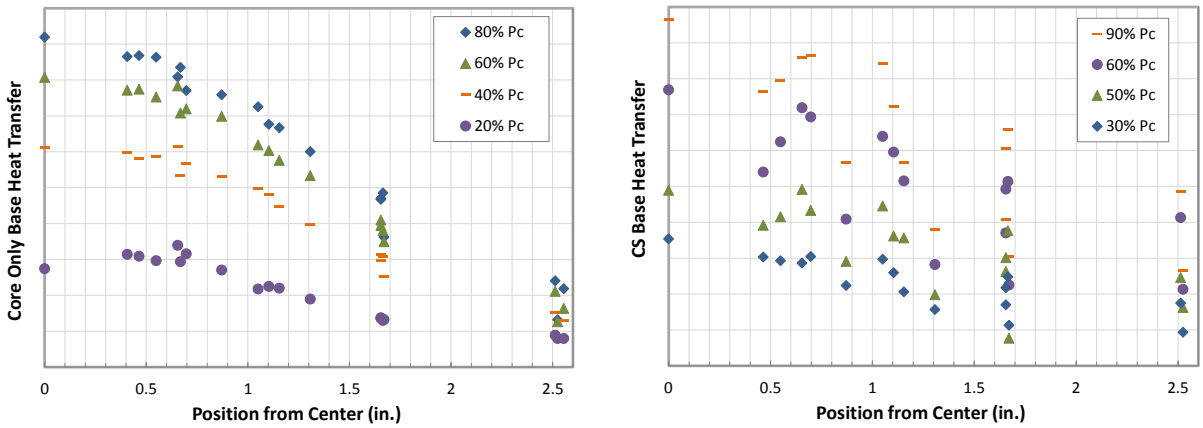

a. Core only heating distribution

b. Full-Stack heating distribution

Figure 18. Rocket Engine/Motor Chamber Pressure Effects on Heating Distribution on Core-Stage Base Plate

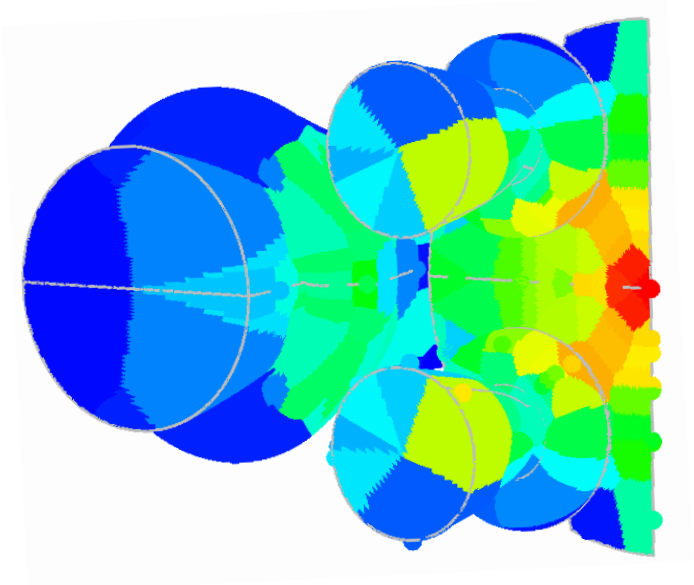

Figure 19. Heat Flux Interpolation of Full-Stack Configuration at 120 kft Condition

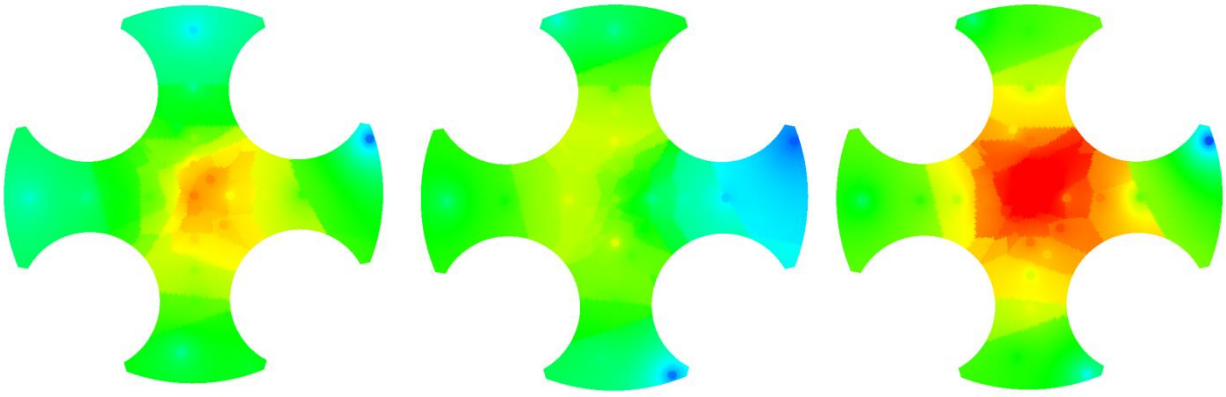

a. 120 kft Condition with 2-deg Gimballed Nozzles (Run 71)

b. 120 kft Condition at 4 deg AoA (Run 62)

c. 120 kft Nominal Condition (Run 64)

Figure 20. Heat Flux Interpolation of Core-Stage Base Plate at 120 kft Nominal and Off-Nominal Conditions

Selection of the steady-state data window was discussed early in this section and all of the data presented so far was based on those steady-state averaged values, but it is important to understand unsteadiness associated with this type of testing and these dynamic fluctuating flow fields. Unsteady heat transfer measurements near the base center from three separate runs are shown below in Figure 21. The core only case without external flow is shown by the dotted red line and is not surprisingly the steadiest. The core only case with flow takes a little longer to stabilize than the no flow case and is more unsteady. The full-stack configuration with flow is the most unsteady, but the average level stabilizes quickly. Results vary but typically base flow stabilizes within five milliseconds of everything reaching pressure. Solid rocket motor chamber pressure differences typically bias the flow slightly from one side to the other with a small bias towards the booster with the lowest pressure. This pressure mismatch likely drives the higher level of unsteadiness shown in Figure 21.

Steady-state base pressure measurements for all of the nominal cases are given in Figure 22. Base pressure measurements at various locations on the core and SRM bases are reported. As with the heat transfer measurements, highest base pressure is typically at the base center, but there's not as much variation as there is with heat flux measurements. Base pressures are needed to help understand base flow physics and guide scaling methodology. SRB1 and SRB2 pressure transducers are both inboard pressure transducers, but they are not at mirrored locations, so pressure values should not match. Figure 22a shows pressure versus altitude, while Figure 22b shows a non-dimensionalized base pressure value versus altitude. As altitude is increased, base pressure spread is larger and the peak non-dimensional value increases due to the changing flow dynamics. Non-dimensional base periphery pressure changes very little.

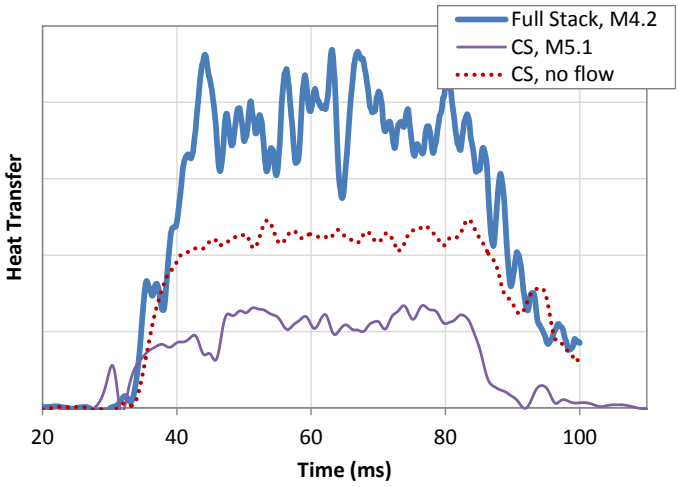

Figure 21. Unsteady Base Heat Transfer Measurements (gauge T84) for Various Configurations & Conditions

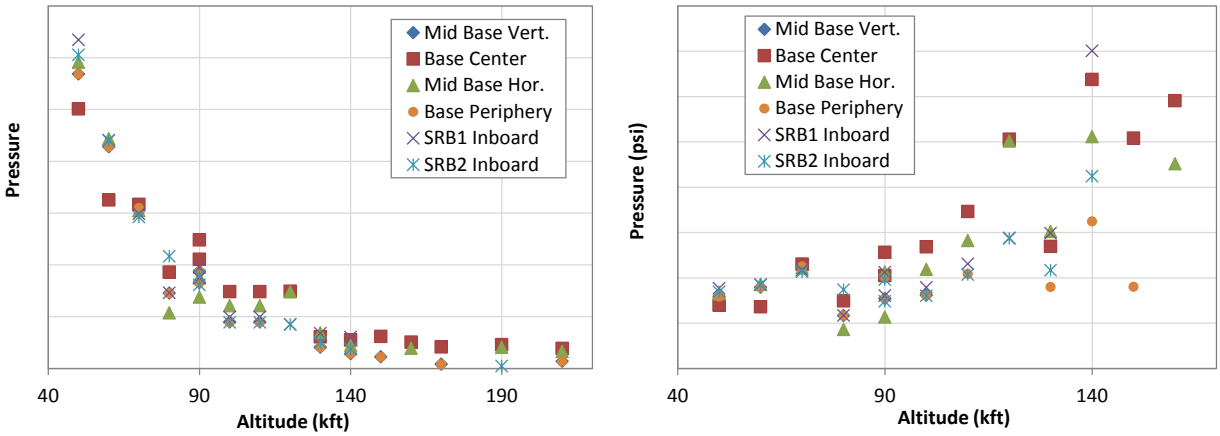

a. Base Pressure b. Normalized base pressure by dynamic pressure

Figure 22. Base Pressure Measurements vs. Altitude for Nominal Conditions

IR Radiometer measurements were only online for twelve runs, but at least some windowed thin-film radiometers were online for every test. The windowed thin-film results are used for adjusting base heat transfer values and are not meant to quantify actual radiative environment, so those results are beyond the scope of this work. IR radiometer results, however, are shown in Figure 23. Most of the runs were for core only configurations, but two full-stack cases are also included within this figure. Data from all four radiometers is shown for each run. The legend describes flow condition, configuration and chamber pressure variances when applicable. Regardless of engine chamber pressure and test section pressure with or without flow, the core only irradiance is fairly constant except at extremely low chamber pressures indicated by the orange circles at about half the other values. As expected, full-stack radiation is significantly higher than core only with about four to five times the radiation measured.

Various images or engines/motors firing are shown in Figure 24. Figure 24a&b show the full-stack configuration firing with Mach 2.8 external flow at approximately 70kft and Mach 4 at 100kft, respectively. Figure 24c shows the core-stage only firing into a simulated altitude of 170kft with no flow. These three images represent the various types of imaging that was captured throughout the test series. Almost all tests included the use of multiple IR imagers and either high-speed video or high-speed Schlieren.

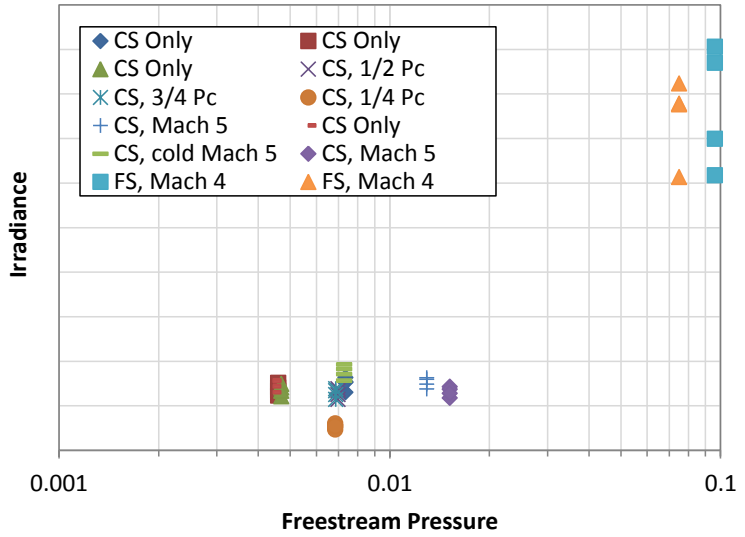

Figure 23. IR Radiometer Measurements vs. Pressure for Various Configurations

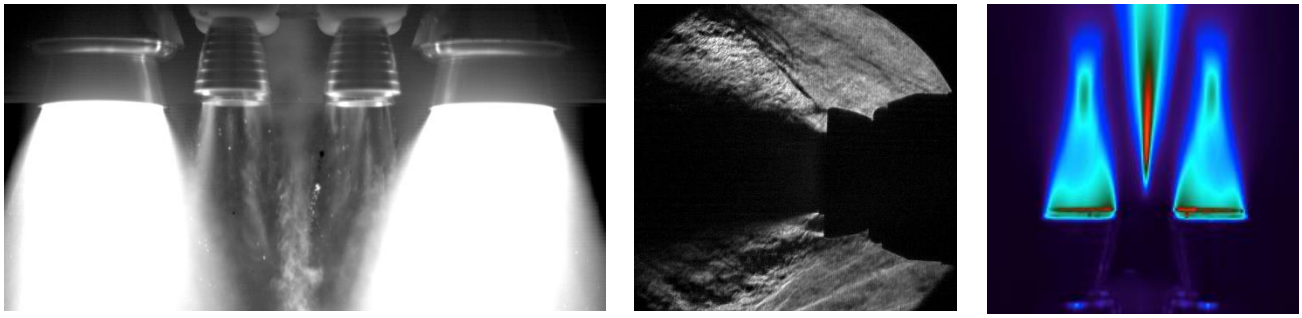

a. Visible camera, top view, 70kft, full-stack

b. Schlieren side view, 100 kft, full-stack

c. Long-wave IR, Top view, 170 kft, Core only

Figure 24. Imaging of 2%-scale SLS hot-fire test at various conditions with full-stack configurations and core-only configuration

V. Conclusion

A sub-scale hot-fire model was developed for NASA MSFC's ATA-002 base heating wind tunnel test. A short-duration test technique is used similar to that used in Space Shuttle and Saturn base heating tests with improvements

to peak chamber pressures and freestream simulation. Rocket motor development, characterization testing, and performance analysis is reviewed showing steady core-stage engine pressures over 2,700 psi and steady solid rocket motor pressures over 700 psi. These operating pressures are nearly twice those achieved in the Space Shuttle base heating program. Additionally, the LENS II shock & Ludwieg tube facility was utilized for testing at or near duplicated flight conditions from Mach 2.8-5.1 with sufficient steady-state test time. Previous base flow plume interaction studies have been done at simulated altitudes in a vacuum chamber or in cold flow facilities where freestream pressure, Mach number, or dynamic pressure could not all be matched simultaneously.

Raw, non-dimensional base heat transfer results are reported for both full-stack and core stage only configurations from 50 kft through 210 kft. Trends for nominal cases show very little heating at 50 kft, with increased heating up to maximum at 120 kft, followed by a slight drop and nearly constant heating above 150 kft. Pre-test predictions and empirical models failed to predict that the engine mount heat shields around the RS-25 nozzle bases have heat fluxes as high as or higher than the base center. Peak inboard solid rocket motor base heating varies with altitude, but values are on the same order of magnitude as the base center, while outboard solid rocket motor base gauges have much lower heating. Freestream total temperatures were duplicated up to the 120 kft condition, and freestream pressures were duplicated at altitudes up to 160-170 kft with tunnel flow and at vacuum only above those altitudes. Altitude simulation alone is likely sufficient at the highest altitudes, but results show increased heating with the higher total temperature freestreams and reduced heating with lower total temperature freestreams in the 150-170 kft range, so freestream enthalpy, and/or dynamic pressure can have a significant effect on measured results. Chamber pressure scaling results show a near linear correlation between base heating values and chamber pressure, indicating ground tests should be completed as close to the flight chamber pressure as possible to minimize uncertainties when scaling data. Off-nominal cases including engine-out runs, gimballed nozzles and angle-of-attack runs all resulted in lower than nominal heating loads on average. SLS base flow dynamics are significantly different from other flight or ground tests, but these tests now provide the data required to adequately define the base thermal environments for the launch vehicle.

Acknowledgements

This work was supported by NASA Marshall Space Flight Center under contract NNJ11HC71C.

References

1. Mehta, M., Knox, K. S., Seaford, C. M., and Dufrene, A. "Space Launch System Base Heating Test: Environments and Base Flow Physics," *54th AIAA Aerospace Sciences Meeting, San Diego, CA*. 2016.
2. Mehta, M., Dufrene, A., Seaford, C. M., Kirchner, R. D., Solly, N., Vizcaino, J., and Kovarik, B. C. "Sub-Scale Space Launch System Core-Stage Rocket Engine Development for Short-Duration Testing," *JANNAF Paper No. 3575, 46th Combustion / 34th Airbreathing Propulsion / 34th Exhaust Plume and Signatures / 28th Propulsion Systems Hazards Joint Subcommittee Meeting*. Albuquerque, NM, 2014.
3. Mehta, M., Dufrene, A., Solly, N., Seaford, C. M., and Kovarik, B. C. "Sub-Scale Space Launch System Solid Rocket Booster Develoment for Short-Duration Testing," *JANNAF Paper no. 3576, 46th Combustion / 34th Airbreathing Propulsion / 34th Exhaust Plume and Signatures / 28th Propulsion Systems Hazards Joint Subcommittee Meeting*. Albuquerque, NM, 2014.
4. Vidal, R. J. "Model Instrumentation Techniques for Heat Transfer and Force Measurements in a Hypersonic Shock Tunnel." Cornell Aeronautical Laboratory Report AD-917-A-1, 1956.
5. Bogdan, L. "High-temperature, Thin-film, Resistance Thermometers for Heat Transfer Measurement." Cornell Aeronautical Laboratory (CAL) Report No. HM-1510-Y-6, February, 1963.
6. Cook, W. J., and Felderman, E. J. "Reduction of Data from Thin-Film Heat-Transfer Gages: A Concise Numerical Technique," *AIAA Journal* Vol. 4, No. 3, 1966, pp. 561-562.
7. Fuller, C. E., Powell, R. T., and Levie, J. K., III. "Diagnostic Evaluation Testing of a Gas Recovery Temperature Probe in the NASA/MSFC Impulse Base Flow Facility." NASA-CR-161500, Remtech, Inc., Huntsville, AL, 1978.
8. Fuller, C. E., W., M. M., Powell, R. T., and Levie, J. K., III. "Utilization of a Gas Temperature Recover Probe on Space Shuttle Short Duration Base Heating Model Tests OH-78 and IH-39." Interim Report M5M8XMS-483101M, Remtech, Inc., Huntsville, AL, 1977.
9. East, R. A., and Perry, J. H. "A Short Time response Stagnation Temperature Probe." Aeronautical Research Council, CP No. 909, 1967.
10. Buttsowrth, D. R., and Jones, T. V. "High Bandwidth Stagnation Temperature Measurements in a Mach 6 Gun Tunnel Flow," *Experimental Thermal and Fluid Science* Vol. 27, 2003, pp. 177-186.
11. Carr, Z., Parker, R., Dufrene, A., and Mehta, M. "Development of a TDLAS Instrument for Plume and Base Temperature Measurements of Sub-Scale Hot-Fire Rockets," *JANNAF Paper No. 3736, 46th Combustion / 34th*

Airbreathing Propulsion / 34th Exhaust Plume and Signatures / 28th Propulsion Systems Hazards Joint Subcommittee Meeting. Albuquerque, NM, 2014.
12. Parker, R., Carr, Z., MacLean, M., Dufrene, A., and Mehta, M. "Space Launch System (SLS) Base Heating Test: Tunable Diode Laser Absorption Spectroscopy," *54th AIAA Aerospace Sciences Meeting, San Diego, CA*. 2016.
13. Dufrene, A., MacLean, M., Wadhams, T., and Holden, M. "Extension of LENS Shock Tunnel Test Times and Lower Mach Number Capability," *53rd AIAA Aerospace Sciences Meeting*. Kissimmee, FL, AIAA 2015-2017, 2015.
14. Wright, M. J., Candler, G. V., and Bose, D. "Data-parallel line relaxation method for the Navier-Stokes equations," *AIAA Journal* Vol. 36, No. Copyright 1998, IEE, 1998, pp. 1603-9.
15. Dufrene, A., MacLean, M., Carr, Z., Parker, R., and Holden, M. "Scaled Rocket Testing in Hypersonic Flow," *20th AIAA International Space Planes and Hypersonic Systems and Technologies Conference* Glasgow, Scotland, AIAA 2015-3550, 2015.